JOURNAL OF MATERIALS SCIENCE 33 (1998) 775–781

Stress corrosion crack propagation in AerMet 100

A. OEHLERT, A. ATRENS
Department of Mining, Minerals and Materials Engineering, The University of Queensland, Brisbane, Qld 4072, Australia

Fracture mechanics tests were carried out for AerMet 100 in distilled water and NaCl (3.5 and 35 g l^{-1}). The initiation period at higher values of the stress intensity factor indicated that load application in the stress corrosion cracking (SCC) environment is a necessary but not sufficient factor for SCC and that time is needed for some other factor (e.g., the local hydrogen concentration) to reach an appropriate value. The threshold stress intensity factor, K_{ISSC}, was found to increase with decreasing NaCl concentration. The plateau stress corrosion crack velocity was 2×10^{-8} m s^{-1} for NaCl (3.5 and 35 g l^{-1}). The fracture mode was transgranular with small areas of an intergranular nature. © *1998 Chapman & Hall*

1. Introduction

In service, stress corrosion cracking (SCC) [1] is often characterized by slow subcritical crack growth at low applied stresses. This means that a metallic component or structure at stresses otherwise considered to be safe can have a growing crack-like defect. Crack initiation and growth can take long periods of time. During the "initiation" period, there may be no outward indication of any defect in the part or structure, which may perform to specification. Nevertheless, while conditions are appropriate, the small subcritical stress corrosion cracks continue to grow in size at low applied stresses until a critical crack size is reached. When the critical crack size is reached, the combination of the crack plus the applied load causes (macroscopic) brittle fracture. This brittle fracture is sudden, often with little prior warning, and can be catastrophic.

SCC often occurs under corrosive conditions where general corrosion is not a problem. The corrosion resistance of interest is caused by surface films that separate the material from its environment. Such films can cause a low rate of general corrosion despite a large thermodynamic driving force for corrosion. For example, stainless steels are stainless because of a very thin passive surface layer which is essentially Cr_2O_3. Although, this layer is so thin (typically less than 4 nm [2–5]) that it cannot be seen with the naked eye, this layer is nevertheless effective in separating the steel from its environment. The passive films on stainless steels are usually self-repairing. The breakdown of such films can be induced chemically (e.g., by chlorides), and pitting corrosion results when the breakdown is localized. Localized film breakdown under the joint action of a stress and an environment is the essence of SCC.

SCC is a complex multistep process [1], in which crack advance occurs by interaction of the applied loading, plastic response of the material at the crack tip, interaction of crack-tip plasticity and surface passive protective films, and localized corrosion in the crack-tip region in a local solution which can be very different from that of the bulk. Crack-tip corrosion can liberate hydrogen which can be involved in the crack advance mechanism by hydrogen embrittlement (HE). Fracture of the surface films can give rise to crack advance by brittle fracture. SCC involves both mechanical factors (such as the stress intensity factor and crack-tip plasticity) and electrochemistry.

SCC is an ongoing concern for high-strength steels in which the susceptibility increases with increasing strength level [6, 7]. Our previous work has dealt extensively with the SCC of high-strength steels. A new test method for SCC was developed [8, 9]; linearly-increasing-stress testing (LIST) was applied to high-strength steels [8, 9] and pure copper [10]. Stress rate effects have been shown [8–11] to be an important part of the SCC mechanism and, in particular, crack-tip creep has been shown to be an important part of the SCC mechanism for high-strength steels undergoing SCC in water [8–11], which can provide [11] an explanation for the stationary stress corrosion cracks observed in service. Room-temperature creep has been measured for high-strength steels including AISI 4340 and AerMet 100 [12] and related to crack initiation [13]. A new model was proposed for SCC for quenched-and-tempered steels based on strain-assisted dissolution [14]. Crack velocity was related to heat treatment and microstructure [15, 16]. The possible causes for the intergranular crack path for high-strength steels undergoing SCC in water have been explored by microstructural characterization using electron microscopy [17–19], measurements of grain-boundary chemistry [20] and electrochemistry [21]. A precipitation-strengthened duplex stainless steel was developed [22].

TABLE I Chemical composition wt %

Element	C	Mn	Si	S	P	Ni	Cr	Co	Mo	Ti	Al	O	N
Amount (wt %)	0.23	0.02	0.01	0.0005	0.003	11.08	3.04	13.40	1.20	0.013	0.004	0.001	0.001

This paper studies the SCC of AerMet 100 in comparison with that of AISI 4340. AerMet 100 is a recently developed high-strength steel with a strength comparable with that of AISI 4340 and with a much higher fracture toughness. AISI 4340 is a high alloy quenched-and-tempered steel [17–19]. AerMet 100 is in contrast a low-C, Fe–Ni lath martensitic alloy which attains its strength through the precipitation of M_2C (M = Mo or Cr) [23–25].

2. Experimental procedure

AerMet 100 was supplied by Carpenter Technology Corporation in the form of a rod of 150 mm diameter. The chemical composition is given in Table I. In the heat treatment a controlled atmosphere furnace with high-purity nitrogen at 125 kPa and a salt bath were used. The heat treatment was as follows: solution treatment for 5 h at 885 ± 5 °C, air cooling to 65 °C in 1.5–2 h, freezing for 1 h at −78 °C in a dry ice–alcohol mixture, ageing for 5 h at 482 ± 2 °C in the salt bath, and air cooling to room temperature. The resulting mechanical properties are given in Table II.

The double-cantilever-beam specimens had dimensions as shown in Fig. 1. They were machined to final dimensions before heat treatment. After heat treatment a slot 35 mm long was cut down the centre-line with a cut-off wheel and the loading holes were machined to their final diameter of 12.5 mm. The fatigue pre-cracking was carried out at 20 Hz using a servo-controlled hydraulic tensile-testing machine under computer control with a constant stress intensity factor amplitude until the fatigue crack length reached a value of a/W between 0.31 and 0.45. During the final stages of fatigue pre-cracking, the maximum stress intensity factor was kept below 65% of that used in the subsequent SCC test. In all cases a fatigue crack 5 mm long was reached after less than 200 000 cycles and fatigue crack initiation required less than 50 000 cycles.

SCC tests were carried out in distilled water and in NaCl (3.5 and 35 $g l^{-1}$) at room temperature unless stated otherwise.

After SCC testing, additional fatigue cracking was carried out to mark the SCC crack clearly. After testing, the specimens were fractured in air and the crack surfaces were examined using scanning electron microscopy (Philips 505). Crack length measurements were carried out with a travelling microscope with an accuracy of ± 0.01 mm

Fig. 2 shows the constant-deflection SCC apparatus. It consisted of two massive plates separated by four stainless steel rods, mounted on a steel frame, and two stainless steel pull rods. One pull rod was attached to a 3 ton load cell whereas a loading nut was used to apply the required deflection via the other pull rod. The signal from the load cell was conditioned in an alternating-current (a.c.) strain amplifier and recorded with a data acquisition system. A glass environment cell surrounded the specimen, sealed with two O-rings located on each of the pull rods. A contact thermometer in the solution was used to control

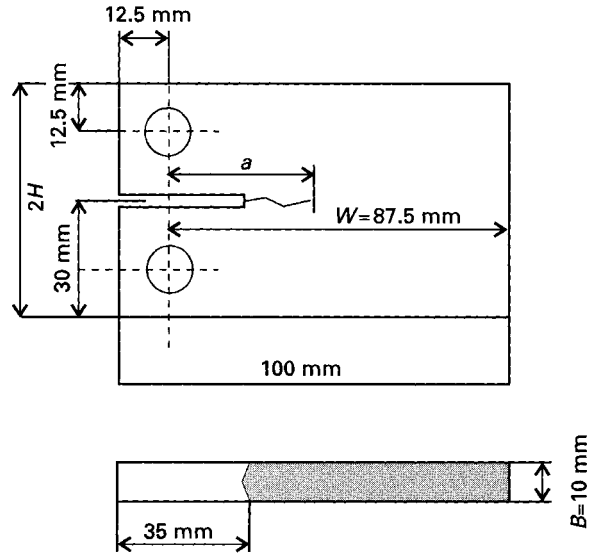

Figure 1 Design and dimensions of the fracture mechanics specimen.

TABLE II Mechanical properties

Rockwell C hardness (HRC)	$\sigma_{0.01}$ % (MPa)	$\sigma_{0.2}$ % (MPa)	Ultimate tensile strength (MPa)
54	1290	1830	2020

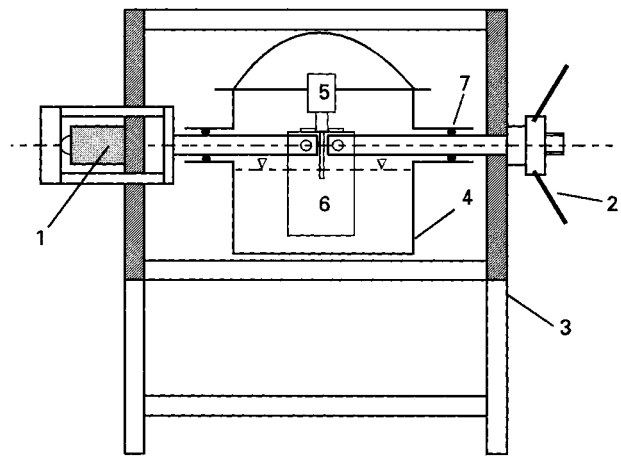

Figure 2 Schematic diagram of the constant-displacement apparatus. 1, load cell; 2, loading nut; 3, frame; 4, environmental cell; 5, COD gauge; 6, double-cantilever-beam specimen; 7, O-rings.

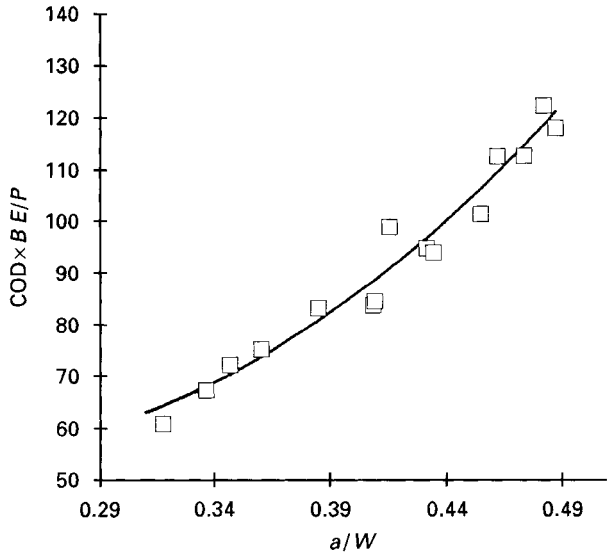

Figure 3 Experimental and calculated compliance calibration for the double-cantilever-beam specimens (10 mm × 100 mm × 60 mm).

the solution temperature via an electric hotplate with electromagnetic stirrer.

The crack-opening displacement (COD), δ_m, was measured during the test using a commercial COD gauge mounted between two knife edges glued to either side of the slot. The COD gauge signal was amplified with an a.c. strain amplifier and recorded with the data acquisition system. The crack length could be obtained from the following experimental compliance calibration which was valid for $0.30 < a/W < 0.5$:

$$\frac{\delta_m BE}{P} = -48.6435\alpha^3 + 973.3497\alpha^2 - 420.6244\alpha - 101.2893 \quad (1)$$

where δ_m(mm) is the crack mouth opening, measured between the knife edges, H(mm) the half-width, B(mm) the specimen thickness in mm, E(MPa) Young's modulus, P(N) the applied load and α the dimensionless crack length equal to a/W. The correlation between the crack length measured on the fracture surface and the crack length measured with Equation 1 was very good as indicated in Fig. 3. Equation 1 was solved numerically for each pair of load and COD measurements allowing evaluation of a/W as a function of time. The stress intensity factor was evaluated from the following calibration [26], which is valid for $0.2 < a/W < 0.45$ [27]:

$$K_L = \frac{Pa}{BH^{3/2}}\left(3.46 + 2.38\frac{H}{a}\right) \quad (2)$$

where P(N) is the applied load and a(mm) is the crack length. The resulting stress intensity factor in N mm$^{3/2}$ is converted to MPa m$^{1/2}$ by dividing by $(1000)^{1/2}$.

3. Stress conversion cracking velocity measurements

Figs 4–8 show typical examples of crack propagation in which the crack length is shown as a function of testing time. For low applied stress intensity factors in region II, the SCC initiated immediately after load application and propagated with a constant rate (Figs 4 and 5), whereas an initiation period could be detected at higher stress intensity factors (Figs 6–8). During

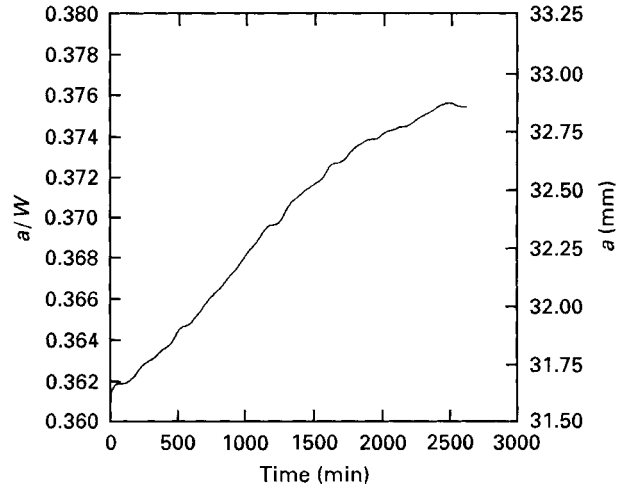

Figure 4 Crack length as a function of time for AerMet 100 in NaCl (3.5 g l^{-1}) at room temperature at 21 MPa m$^{1/2}$.

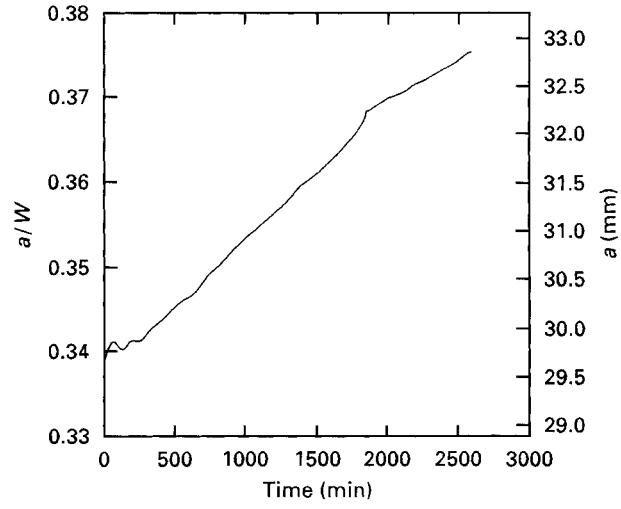

Figure 5 Crack length as a function of time for AerMet 100 in NaCl (3.5 g l^{-1}) at room temperature at 24.4 MPa m$^{1/2}$.

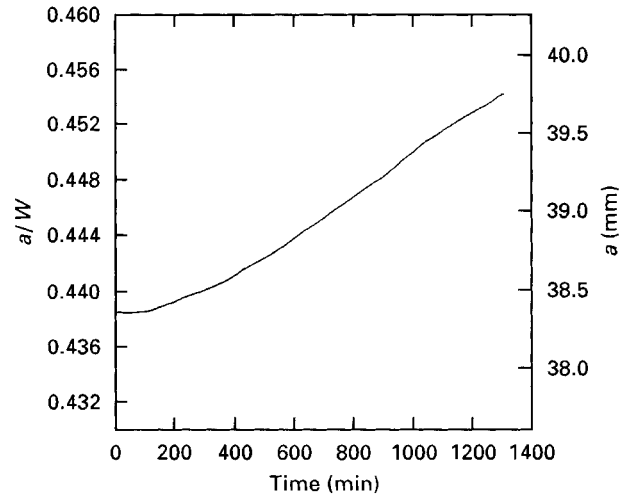

Figure 6 Crack length as a function of time for AerMet 100 in NaCl (35 g l^{-1}) at room temperature at 35 MPa m$^{1/2}$.

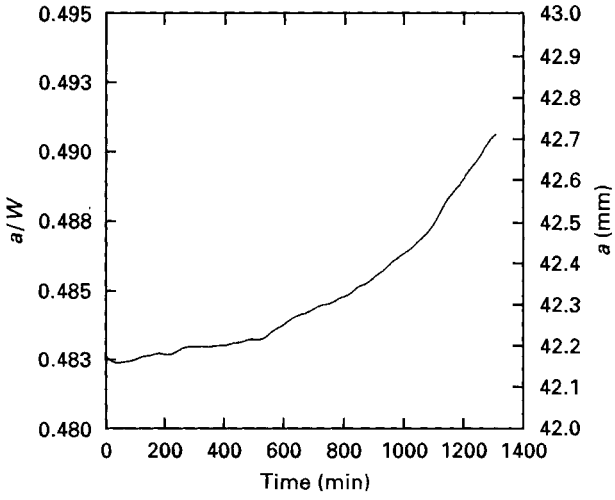

Figure 7 Crack length as a function of time for AerMet 100 in NaCl (3.5 g l^{-1}) at room temperature at 63 MPa $m^{1/2}$.

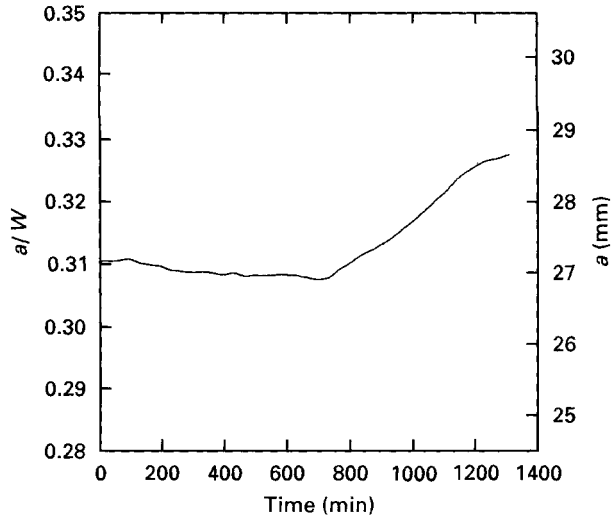

Figure 8 Crack length as a function of time for AerMet 100 in NaCl (35 g l^{-1}) at room temperature at 38.5 MPa $m^{1/2}$.

this initiation period, the stress corrosion crack started to propagate and its propagation rate accelerated until it reached a steady value. This steady-state value was taken as the SCC velocity in Fig. 9. For the specimen in Fig. 8, no crack propagation was detected during the first 750 min, after which the crack velocity was approximately constant at 4.5×10^{-8} m s^{-1}.

The SCC velocity is shown in Fig. 9 as a function of the applied stress intensity factor; the steady-state value was taken as the SCC velocity. No SCC was observed in distilled water in separate tests lasting 24 h at 30 (two tests), 38, 43 and 51 MPa $m^{1/2}$. Similarly, there was no SCC in 100 h and 24 h, respectively, for two specimens, loaded at 14.9 and 18.4 MPa $m^{1/2}$ in NaCl (3.5 g l^{-1}) at room temperature. In contrast there was SCC for two specimens loaded for 10 days in NaCl (35 g l^{-1}) at 14.6 MPa $m^{1/2}$ and 17.4 MPa $m^{1/2}$, with average crack velocities equal to 4.1×10^{-10} m s^{-1} and 8.3×10^{-10} m s^{-1}, respectively. All other specimens, with one exception, exhibited crack propagation corresponding to region II as shown in Fig. 9. One specimen, loaded at 57 MPa $m^{1/2}$ in NaCl (3.5 g l^{-1}) did not experience

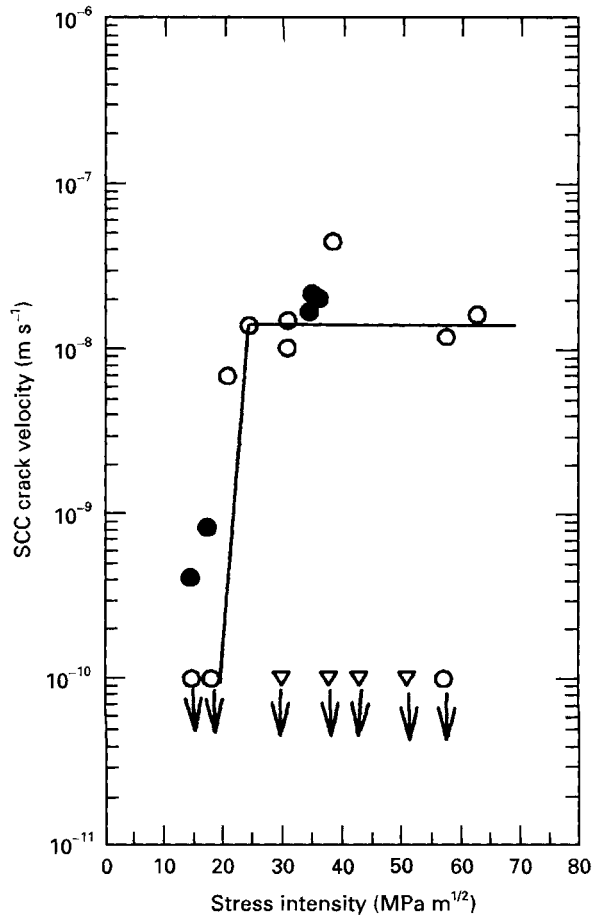

Figure 9 Stress corrosion crack velocity for AerMet 100 in distilled water (▽), in NaCl (3.5 g l^{-1}) (○) and in NaCl (35 g l^{-1}) (●).

SCC in 1830 min; it was again fatigue pre-cracked and reloaded in the same solution at 58 MPa m^{-1}; then SCC started immediately after load application.

The plot of average crack velocity as a function of the applied stress intensity factor (Fig. 9) is typically divided into stages I and II. The stage II or plateau crack velocity was 2×10^{-8} m s^{-1} and exhibited a relatively small scatter within a factor of two, independent of NaCl concentration, which was in contrast with the influence of NaCl concentration on K_{ISCC}.

4. Fractography

The transition between the fatigue pre-crack and SCC was very sharp in the form of a straight line over the whole specimen width (Fig. 10). The stress corrosion crack morphology was predominantly transgranular (Fig. 11), with some areas appearing intergranular (Figs 12 and 13), particularly the secondary cracks (Fig. 13) which were most often observed at the start of the stress corrosion cracks.

A typical specimen cross-section is illustrated in Fig. 14; the SCC initiated at a distance of 1.25 mm from the specimen edge with no SCC at the specimen centre. With increasing time, the SCC extended over the whole specimen width and developed the typical shape depicted in Fig. 14 with the crack length at the specimen centre about 1 mm less than the longest crack length. Cracks which had propagated less than

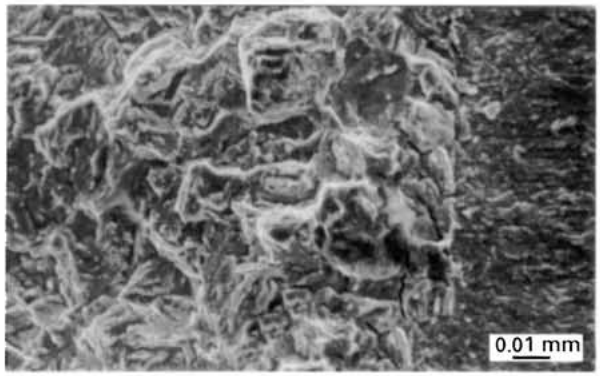

Figure 10 Transition between fatigue (right) and SCC (left) in NaCl (3.5 $g l^{-1}$).

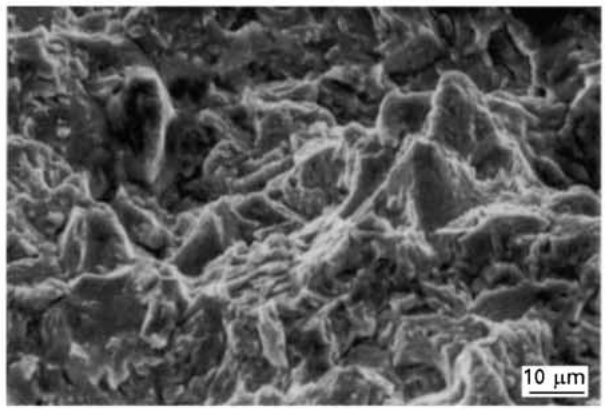

Figure 11 Transgranular SCC.

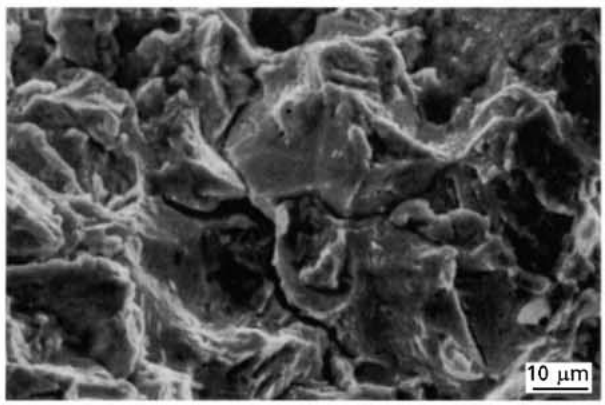

Figure 12 Area with intergranular SCC.

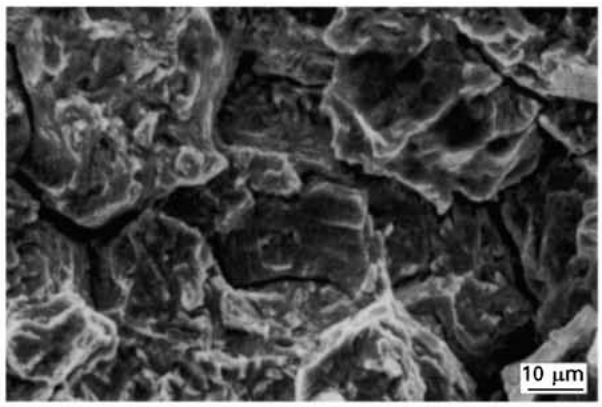

Figure 13 Area with intergranular secondary SCC.

Figure 14 Curved stress corrosion crack front which was observed on all AerMet 100 specimens in NaCl at room temperature.

1 mm had not extended over the whole specimen width.

There was no significant change in fractography with stress intensity factor or with NaCl concentration.

5. Discussion

Figs 4–8 showed that there was an initiation period at higher stress intensity factors (Figs 6–8) whereas, for low applied stress intensity factors in region II, the SCC initiated immediately after load application and propagated with a constant rate (Figs 4 and 5). During this initiation period, the stress corrosion crack started to propagate and its propagation rate accelerated until it reached a steady value. This seems to indicate that load application in the SCC environment is a necessary but not sufficient factor for SCC and that, at higher stress intensity factors, time is needed for some other factor to reach an appropriate value. An obvious candidate is the production and/or accumulation of hydrogen concentration in the crack-tip area which would be consistent with the widely held view that HE is involved in the mechanism for SCC of high-strength steels [28]. The hydrogen source could be internal inside the metal, or hydrogen could enter the metal after liberation at the crack tip by a localized corrosion reaction. If hydrogen is from a localized crack-tip corrosion reaction, then the requirement for crack-tip strain can be understood in terms of rupture of a protective film which exposes the crack tip to the electrolyte and allows corrosion to occur.

The stress corrosion crack path was observed to be mainly transgranular with some areas showing intergranular features. This is in contrast with SCC of high-strength steels such as AISI 4340 where SCC is predominantly intergranular. This indicates that the details of the crack propagation mechanism are different for AerMet 100 and AISI 4340.

Fig. 15 compares the SCC behaviour of AerMet 100 as measured in the present work (from Fig. 9) with literature data for AISI 4340 [7]. Similar threshold stress intensity factors were observed for both steels. However, the plateau crack velocity of AerMet 100 is two orders of magnitude lower than that of AISI 4340 despite the lower yield strength of AISI 4340;

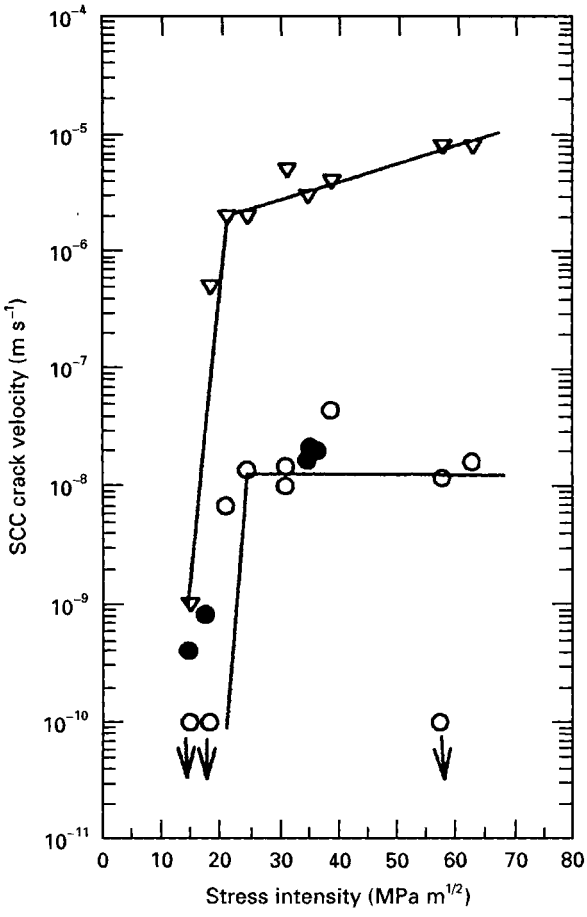

Figure 15 Comparison of SCC behaviour of AerMet 100 in NaCl (3.5 g l^{-1}) (○) and in NaCl (35 g l^{-1}) (●) at $\sigma_{0.2}$ = 1890 MPa and room temperature with that of AISI 4340 in distilled water at $\sigma_{0.2}$ = 1700 MPa and 23 °C [7] (▽).

increased yield strength usually results in a strong increase in plateau crack velocity [6, 7]. This provides a further indication that the details of the crack propagation mechanism are different for AerMet 100 and AISI 4340. Furthermore, the plateau SCC velocity for AerMet 100 was the same in NaCl at both 3.5 and 35 g l^{-1}.

The threshold stress intensity factor, K_{ISCC}, for AerMet 100 increased with decreasing NaCl concentration; SCC was observed at 14.6 MPa m^{-1} at an NaCl concentration of 35 g l^{-1}; no SCC was observed until above 18.4 MPa $m^{1/2}$ at an NaCl concentration of 3.5 g l^{-1} and no SCC was observed in distilled water even at 51 MPa $m^{1/2}$. These observations allow estimates to be made for values of K_{ISCC} as summarized in Table III. The decrease in K_{ISCC} with NaCl concentration is attributed to increased NaCl concentrations, leading to easier breakdown of the protective film at the crack tip and thereby facilitating SCC at a lower value of the stress intensity factor. This is consistent with observations on the initiation of SCC with smooth specimens [13] where SCC initiation was associated with strain-assisted breaking of a surface film. Although these experiments suggest the importance of a surface film in the SCC mechanism, the propagation mechanism could indeed be HE as argued above. The importance of a surface film indicates that it might be possible to develop from AerMet 100 a high-strength

TABLE III Values of the threshold intensity factor, K_{ISCC}, for AerMet 100 in different environments

Environment	K_{ISCC} (MPa $m^{1/2}$)		
	This work	Neu [29], 10 000 h	Neu [29] 1000 h
Distilled water	>52		
NaCl (3.5 g l^{-1})	19		
NaCl (35 g l^{-1})	≈14	23	32

high-toughness steel with a very high resistance to SCC (i.e., $K_{ISCC} \rightarrow K_{IC}$) by increasing the quality of its passivity by for example alloying to much higher Cr levels as was done in the development of a precipitation-strengthened duplex stainless steel [22].

Table III compares the results for K_{ISCC} from the present work with literatures values [29]. Neu [29] evaluated K_{ISCC} from the final stress intensity factor at the tip of a stress corrosion crack for constant-displacement fracture mechanism specimens exposed for long time periods to 3.5% NaCl. On exposure of such specimens, the stress intensity factor at the crack tip decreases as the stress corrosion crack grows in length. As K_{ISCC} is approached, the crack velocity decreases by orders of magnitude; therefore, at best, K_{ISCC} is only approached asymptotically and very long testing times are needed. Furthermore, situations when stress corrosion cracks grow into regions of decreasing applied stress intensity can lead to crack arrest for applied stress intensity factors considerably above K_{ISCC} [11].

6. Conclusions

Fracture mechanics tests of AerMet 100 in distilled water and NaCl (3.5 and 35 g l^{-1}) revealed the following.

1. The initiation period at higher values of the stress intensity factor indicated that load application in the SCC environment is a necessary but not sufficient factor for SCC and that time is needed for some other factor (e.g., the local hydrogen concentration) to reach an appropriate value.
2. The threshold stress intensity factor, K_{ISCC}, increased with decreasing NaCl concentration.
3. The plateau stress corrosion crack velocity was 2×10^{-8} m s^{-1} for NaCl (3.5 and 35 g l^{-1}).
4. The fracture mode was transgranular with small areas of an intergranular nature.

Acknowledgement

J. Dahl of Carpenter Technology Corporation is thanked for the supply of the AerMet 100.

References

1. A. ATRENS and Z. F. WANG, *Mater. Forum* **19** (1995) 9.
2. S. JIN and A. ATRENS, *Appl. Phys. A* **42** (1987) 149.
3. *Idem., ibid.* **50** (1990) 287.
4. A. S. LIM and A. ATRENS, *ibid.* **53** (1992) 273.

5. *Idem., ibid.* **54** (1992) 500.
6. M. O. SPEIDEL, in "Corrosion in power generating equipment", edited by M. O. Speidel and A. Atrens (Plenum, New York, 1984) p. 85.
7. R. MAGDOWSKI PEDRAZZOLI and M. O. SPEIDEL, in Parkins Symposium on Fundamental Aspects of Stress Corrosion Cracking, edited by S. M. Bruemmer, E. I. Meletis, R. H. Jones, W. W. Gerberich, F. P. Ford and R. W. Staehle (Metallurgical Society of AIME, Warrendale, PA, 1992) p. 341.
8. A. ATRENS, C. C. BROSNAN, S. RAMAMURTHY, A. OEHLERT and I. O. SMITH, *Measurement Sci. Technol.* **4** (1993) 1281.
9. S. RAMAMURTHY and A. ATRENS, *Corros. Sci.* **34** (1993) 1385.
10. J. SALMOND and A. ATRENS, *Scripta Metall. Mater.* **26** (1992) 1447.
11. R. M. RIECK, A. ATRENS and I. O. SMITH, *Metall. Trans. A* **20** (1989) 889.
12. A. OEHLERT and A. ATRENS, *Acta Metall. Mater.* **42** (1994) 1493–1508.
13. *Idem., Mater. Forum* **17** (1993) 415.
14. A. ATRENS, R. M. RIECK and I. O. SMITH, in "Advances in fracture research", Proceedings of the 7th International Conference in Fracture, edited by K. Salama, K. Ravi-Chandar, D. M. R. Taplin and P. Rama Rao (Pergamon, Oxford, 1989) pp. 1603–1609.
15. R. M. RIECK, A. ATRENS and I. O. SMITH, *Mater. Forum* **13** (1989) 48.
16. *Idem., ibid.* **13** (1989) 54.
17. J. D. GATES, A. ATRENS and I. O. SMITH, *Z. Werkstoftech.* **18** (1987) 165.
18. *Idem., ibid.* **18** (1987) 179.
19. *Idem., ibid.* **18** (1987) 344.
20. J. SKOGSMO and A. ATRENS, *Acta Metal. Mater.* **42** (1994) 1139.
21. S. RAMAMURTHY, A. ATRENS and I. O. SMITH, *Mater. Sci. Forum* **44–45** (1989) 139.
22. A. ATRENS, R. COADE, J. ALLISON, H. KOHL, G. HOCHOERTLER and G. KRIST, *Mater. Forum* **17** (1993) 263.
23. R. M. HEMPHILL and D. E. WERT, US Patent 5087415 (1992).
24. G. R. SPEICH, *Metall. Trans.* **4** (1973) 303.
25. P. M. NOVOTNY and J. M. DAHL, in Proceedings of the 32nd Mechanical Working and Steel Processing Conference (ISS Warrendale, PA, 1991) 275.
26. H. R. SMITH and D. E. PIPER, in "SCC in high strength steels and in titanium and aluminium alloys", edited by B. F. Brown (Naval Research Laboratory, Washington, DC, 1972) p. 17.
27. R. EHLERS and J. DENK, *Mater. Tech.* **4** (1984) 127.
28. P. G. MARSH and W. W. GEBERICH, in "Stress corrosion cracking, materials performance and evaluation", edited by R. H. Jones (American Society for Metals, Metals Park, OH, 1992) p. 63.
29. E. NEU, Naval Aircraft Warfare Centre, Aircraft Division, Warminster, PA.

Received 24 June 1996
and accepted 20 August 1997